

Assessment of tomography signals in view of neural network reconstruction at ISTTOK

R. V. Cardoso, D. R. Ferreira, D. D. Carvalho, D. Hachmeister, H. Fernandes, H. Alves and H. Figueiredo

*Instituto de Plasmas e Fusão Nuclear, Instituto Superior Técnico, Universidade de Lisboa
1049-001 Lisboa, Portugal*

E-mail: ruben.cardoso@tecnico.ulisboa.pt

ABSTRACT: The detector measurements that serve as a basis for the tomographic reconstruction of plasma radiation profiles can be affected by a number of issues. In this work, we are especially concerned about reflections inside the vessel that appear as direct incidences, when in fact those contributions come from points that are outside the line of sight of a detector. This problem occurs in devices such as ISTTOK, where the surface of the inner vessel acts as an optical system capable of reflecting light. To assess the contribution of those reflections to the detector signals, we used an experimental setup comprising a cylindrical gas-discharge lamp placed at several radial and angular positions inside the vessel. As detectors, we used two photodiode arrays, one placed on the equatorial plane and the other at the top of the vessel. At the same time, we modelled this experimental setup in a ray-tracing simulation software so that, once the experimental data agrees with the simulation data, we can use this simulated environment to study the effect of reflections in realistic plasma profiles. When properly calibrated, such simulated environment can be used to generate large volumes of high-quality data to train a neural network for plasma tomography.

KEYWORDS: Plasma Tomography; Ray-tracing; Reflections

1 Introduction

Plasma tomography consists in reconstructing the plasma emissivity profile on a poloidal cross-section of a fusion device, based on measurements of the integrated emissivity along multiple lines of sight. The main challenge for this tomographic reconstruction is the ill-posedness of the problem: the number of available lines of sight is typically much lower than the total number of pixels in the reconstruction. Several methods have been developed to deal with this issue [1]. However, typically these algorithms require long computation times that are not compatible, for example, with real-time applications such as plasma position control [2].

Furthermore, these methods do not take into account complex viewing geometries, effects such as occlusion and vignetting that arise due to the use of pinhole cameras, and radiation reflections on the vessel walls, which are interpreted as direct incidences coming from elsewhere in the plasma and cause emission artefacts along wall surfaces, degraded localisation and background halos [3].

Recent approaches use deep neural networks to achieve similar results in a fraction of the time, which enables the use of tomography for real-time control applications [1]. Nonetheless, these reconstructions are unable to outperform the algorithms used to obtain the training data, and all the artefacts or inaccuracies arising from the use of those algorithms affect the neural network results. Therefore, it is important to improve the quality of the training data in order to achieve very fast reconstructions that take into account the previously mentioned effects.

In this work, developed at ISTTOK, we assess the contribution of reflections to the detector signals and create a ray-tracing simulation of the tomography diagnostic, which allows us to obtain the simulated detector signals for any desired profile. This simulation enables an accurate understanding of the problem geometry, and the generation of high-quality data to train neural networks for plasma tomography.

2 Experimental setup

The tomography diagnostic at ISTTOK consists of two pinhole cameras placed at the top and at the low-field side of the tokamak. Each camera is composed of 16 photodiodes sensitive from the infrared to soft X-rays, and the pinhole placed in front of the photodiode array defines the line of sight for each detector. Some examples of rays with direct incidence on the detectors are illustrated in Figure 1(a).

Experimental data was collected with two main purposes: analysing the importance of reflections on the total power received by each camera, and serving as spatial calibration data to fine-tune the simulation geometry and vessel roughness.

A cylindrical cold cathode lamp with 4.1mm of diameter was placed at various radial and poloidal positions inside the tokamak vessel, with the help of a 3D-printed support structure shown in Figure 1(b). The detector measurements were acquired for a total of 57 different positions of the lamp, as shown in Figure 1(c), using angle increments of 45° for 3 cm radius, and 15° for 5 cm and 7 cm radii. Since the lamp was used in strobe mode, a total of 5 sets of detector measurements were obtained for each position.

To obtain a relation between the power received by the different detectors, their signals were integrated during 7×10^{-3} s, starting from the instant of maximum lamp emissivity. An average of

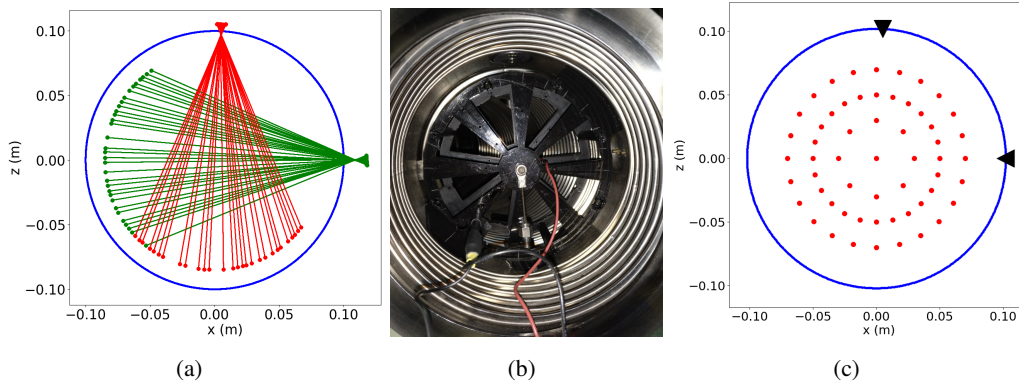


Figure 1: (a) Examples of rays with direct incidence on the detectors. (b) Lamp support structure inside vessel. (c) Lamp placement positions (red) and camera's pinholes positions (black triangles).

these integrals over the 5 sets of measurements yielded the final value taken for each detector, hence decreasing the variability arising from small changes in the lamp emissivity. Finally, these values were normalised by a single constant in order to scale them to approximately 1, while maintaining their relations.

3 Effect of reflections

The collected experimental data allowed the study of reflections on the vessel walls. There are two distinct types of reflections: diffuse, which are independent of the incidence angle and whose power depends only on a material constant; and specular, which are mirror-like reflections depending on the angle between the ideally reflected ray, the incident light vector and a material constant [4].

Diffuse reflections introduce noise in tomographic reconstructions due to their small but random influence over the different detectors. On the other hand, specular reflections have a greater impact because these can be misinterpreted as direct incidences. Examples of such reflections are represented in Figure 2(a) and the corresponding detector measurements are shown in Figure 2(b). The relevance of specular reflections can be seen in detectors 11 and 12 of the outer camera and the

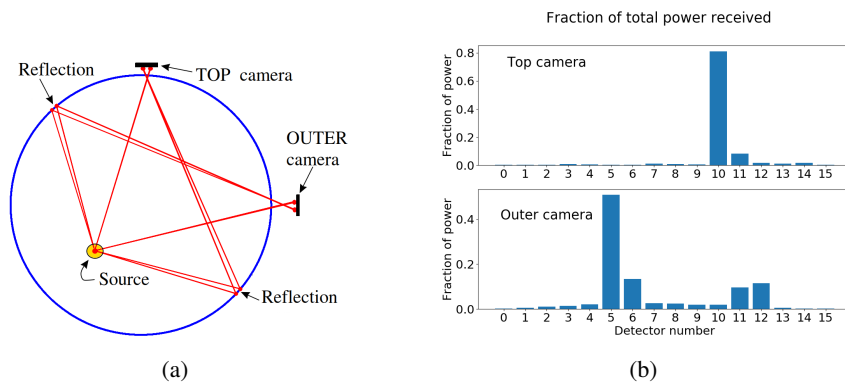


Figure 2: (a) Lamp (yellow) and emitted rays that reach a detector (red). (b) Normalised signals obtained for the lamp placement shown in Figure 2(a).

effects of diffuse reflections are clear on detectors 1 to 4 and 7 to 10. Note that detector numbering goes from left to right for the top camera, and up to down for the outer camera.

An analysis of the reflections obtained for all lamp positions allowed the determination of the fraction of total power received by each camera that is due to the two types of reflections. For each camera and every lamp position, the average, μ , and standard deviation, σ , of the 10 least intense detector measurements were calculated. Then, a 4σ threshold was defined. All the detectors whose measurements were below this threshold were considered diffuse reflections. For the remaining detectors, the one with the most intense measurement was considered a direct incidence, as well as its two contiguous detectors if they were above the threshold. The remaining detectors above 4σ were considered specular reflections.

The results are shown in Table 1. About 90% of the tested positions show the existence of specular reflections. Additionally, the contribution of reflections towards the total received power is not negligible and, although usually less than 10%, can reach values up to 40%.

Table 1: Fraction of total power received by each camera due to each type of reflection.

	Top camera	Outer camera
Specular	7.5%	8.0%
Diffuse	5.9%	10.9%

4 Ray-tracing simulation

The experimental setup was modeled using a ray-tracing simulation environment based on the Python package Raysect [5]. This simulation environment has been previously used to model the bolometer system of ASDEX Upgrade [6], and is capable of accurately describing and simulating the tomography diagnostic of ISTTOK. For this purpose, we developed a 3D model for the vessel and for the pinhole cameras. These models were created with the help of SketchUp software and used the precise dimensions of the original structures, obtained through careful measurements and consulting of the technical drawings.

The final 3D models were uploaded to the simulation environment and placed with millimetric precision on their relative positions. The detector arrays were then placed in the appropriate positions, replicating their sizes and spacing as described in the datasheet. The materials chosen for the components were also carefully selected: the cameras were approximated as perfect absorbers, which is a realistic assumption and speeds up the simulations by preventing the computation of irrelevant rays; and the vessel, which is composed of the nickel-chromium-based superalloy Inconel, was approximated as a nickel surface, allowing a good modelling of the reflected, transmitted and absorbed power.

Given the sensitivity of the results to the geometry of the simulation, an extra step of spatial calibration was required. To achieve this fine-tuning of the setup geometry, a uniform volume emitter with the dimensions of the cold cathode lamp was placed in the same 57 positions for which the experimental data was obtained. To ensure the best possible replication of the real setup in the simulation and, consequently, ensure the best geometry calibration, the lamp support structure was also taken into account in the simulation. These additional components are relevant because

they can block or obscure the camera pinholes. This way, it was possible to compare the real and simulated detector measurements and manually adjust the pixel and camera positions to achieve the best matching between them.

However, given the uncertainties associated with the placement of the lamp in the experimental setup, it is impossible to achieve a perfect matching for all the 57 lamp positions. Therefore, to achieve the best possible matching, a loss function (L_{geo}) was defined to evaluate the similarity between the real and simulated data for the 32 detectors across all 57 positions. This function is defined by the following expression, where n_{pos} is the number of lamp positions and n_{det} is the number of detectors,

$$L_{\text{geo}} = \sum_{p=1}^{n_{\text{pos}}} \sum_{s=1}^{n_{\text{det}}} |P_{\text{real}}(p, s) - P_{\text{simul}}(p, s)| \quad (4.1)$$

where P_{real} and P_{simul} correspond to the real and simulated power collected by each detector. An L1 norm was used to ensure that the minimization takes into account the less intense measurements corresponding to reflections; an L2 norm, for example, would grant much greater importance to the direct incidences due to their most intense measurements, neglecting the reflections. The position and the tilt of the detectors arrays relative to the pinhole were found to be critical parameters with the most impact in the simulations. Two grid searches - one for the top camera and another for the outer camera - were performed in order to find the best values for those parameters, i.e. the values that minimised the loss function above. The final positions correspond to a Pearson correlation coefficient between the real and simulated detector measurements of 0.85 for the top camera and 0.83 for the outer camera.

The last parameter to be tuned was the vessel roughness. This parameter controls the relation between specular and diffuse reflections on the vessel walls, with 0 being perfectly specular and 1 being perfectly rough. To achieve that, a new loss function was defined

$$L_{\text{rough}} = \sum_{p=1}^{n_{\text{pos}}} \sum_{s \in \text{detectors with specular reflections}} |P_{\text{real}}(p, s) - P_{\text{simul}}(p, s)| \quad (4.2)$$

This loss is similar to the previous one in (4.1) but, instead of summing over all detectors, it sums only over those detectors that, for each lamp position, show the effect of specular reflections on their received power. These reflections are highly directional and, therefore, only reach 2 or 3 detectors for each lamp position. Only these detectors were considered because varying the vessel roughness greatly affects the power collected due to specular reflections; thus, the measurements of such detectors are the best indicators for the effects of roughness changes. By minimizing the difference between real and simulated power, the vessel roughness was tuned to match the real data. This loss function was computed for several possible values of roughness and 0.23 was taken as the appropriate value.

Furthermore, Raysect offers the possibility of creating custom volume emitters by setting the emissivity of points inside a given region. This way, a cylinder was placed inside the simulated vessel and the emissivity of each point inside this cylinder was defined with the help of a generic synthetic plasma profile generator. This tool is able to generate emissivity profiles with any desired shape by stacking generic contour shapes according to a list of possible functions, such as gaussian, quadratic or generalised bell functions.

5 Results

The ray tracing simulation combined with the generic synthetic plasma profile generator allowed for the generation of any desired plasma emissivity profile and computation of its corresponding simulated detector measurements. For the profile in Figure 3(a), a comparison between the detector signals corresponding to the ray-tracing simulation and those obtained through simple emissivity integration along the lines of sight (LoS) is shown in Figures 3(b) and 3(c). As expected, the differences are considerable. Detectors whose measurements were null because their lines of sight did not cross any plasma, now present signals caused by reflections, which considerably change the power distribution throughout the various detectors.

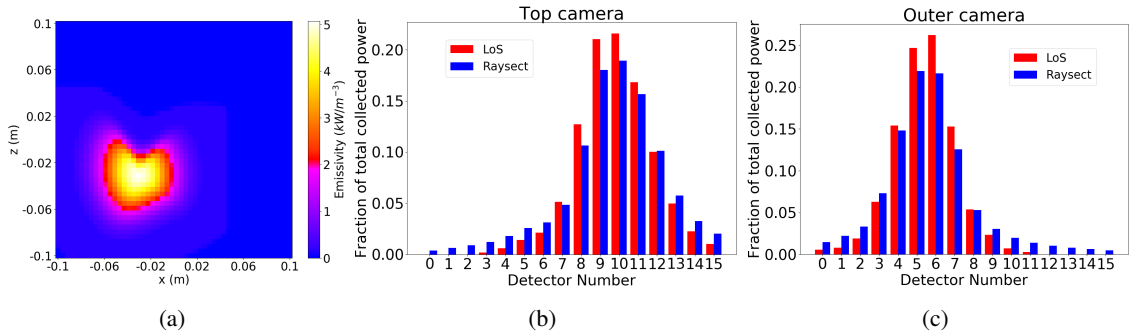


Figure 3: (a) Example of plasma profile. (b) Simulated signals for the top camera. (c) Simulated signals for the outer camera.

The pairs (detector measurements, plasma emissivity profile) obtained with the ray-tracing simulation were used as features and targets for the training of a transposed convolutional neural network. The 32 detector measurements were used as the network inputs and the outputs consisted of the corresponding emissivity profiles discretised into a 60×60 pixel grid. Similarly to previous works [7], a mean absolute error loss function was used to compare the training and predicted profiles throughout the training process. The trained network was able to learn the data and yield accurate reconstructions of training emissivity profiles. Figures 4(a) and 4(b) show the reconstruction of an example training profile.

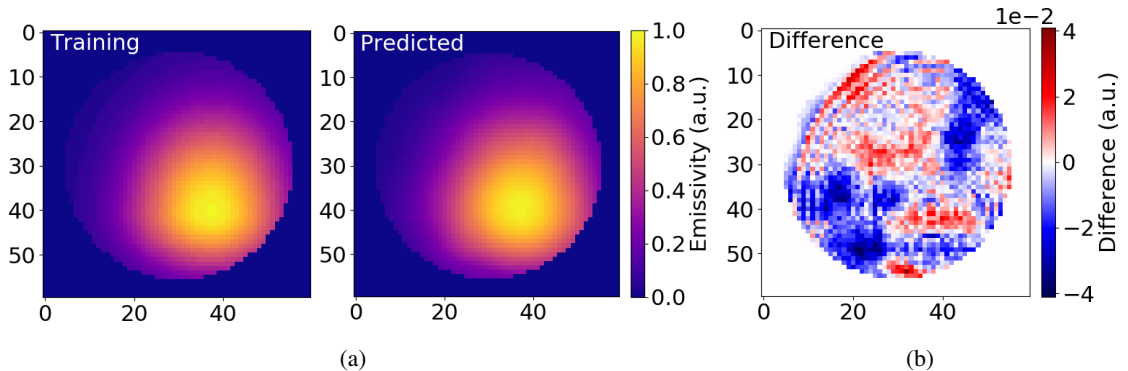


Figure 4: (a) Example of training plasma emissivity profile and corresponding reconstruction using the neural network. (b) Difference between training and predicted emissivity profiles.

Acknowledgments

IPFN activities received financial support from *Fundação para a Ciência e Tecnologia* through project UID/FIS/50010/2019.

References

- [1] J. Mlynar, T. Craciunescu et al., *Current research into applications of tomography for fusion diagnostics*, *Journal of Fusion Energy* **38** (2019) 458–466.
- [2] P. J. Carvalho, *Tomography Algorithms for Real-Time Control in ISTTOK*. PhD thesis, Instituto Superior Técnico, 2010.
- [3] J. Karhunen, M. Carr et al., *Effect of reflections on 2D tomographic reconstructions of filtered cameras and on interpreting spectroscopic measurements in the JET ITER-like wall divertor*, *ECPD 2019* (2019) .
- [4] M. Odstrčil, J. Mlynář et al., *Plasma tomographic reconstruction from tangentially viewing camera with background subtraction*, *Review of Scientific Instruments* **85** (2014) 013509.
- [5] A. Meakins and M. Carr, *raysect/source: v0.5.2 release (version v0.5.2)*, *Zenodo* (August, 2018) .
- [6] M. Carr, A. Meakins and Others, *Description of complex viewing geometries of fusion tomography diagnostics by ray-tracing*, *Review of Scientific Instruments* **89** (2018) 083506.
- [7] D. Carvalho, D. Ferreira, P. Carvalho, M. Imrisek, J. Mlynar, H. Fernandes et al., *Deep neural networks for plasma tomography with applications to JET and COMPASS*, *Journal of Instrumentation* **14** (sep, 2019) C09011–C09011.